

Phase transformation mechanism between γ - and θ -alumina

Shu-Hui Cai,^{1,2} Sergey N. Rashkeev,³ Sokrates T. Pantelides,³ and Karl Sohlberg^{2,*}

¹*Department of Physics, State Key Laboratory for Physical Chemistry of Solid Surface, Xiamen University, Xiamen 361005, People's Republic of China*

²*Department of Chemistry, Drexel University, Philadelphia, Pennsylvania 19104, USA*

³*Department of Physics and Astronomy, Vanderbilt University, Nashville, Tennessee 37235, USA and Solid State Division, Oak Ridge National Laboratory, Oak Ridge, Tennessee 37831, USA*

(Received 4 November 2002; revised manuscript received 12 February 2003; published 16 June 2003)

γ -alumina transforms to θ -alumina and finally to α -alumina in the sequence of thermal dehydration of boehmite. We report a detailed theoretical investigation of the γ to θ -alumina transformation based on first-principles density-functional calculations. Although the *unit* cells of cubic γ -alumina and monoclinic θ -alumina look quite different, we have identified cells for both the polytypes (with the composition $\text{Al}_{16}\text{O}_{24}$) that look very similar and can be continuously transformed one to another. The transformation may be described by a set of aluminum atom migrations between different interstitials while the oxygen atoms remain fixed. Total-energy calculations along the paths of the atomic migrations have been used to map out possible transformation pathways. The calculated conversion rate accurately predicts the experimentally measured transformation temperature. The deduced orientation relationships between the γ - and θ -alumina forms also agree with experimental observations. The formation of several different interfaces observed in domain boundaries of θ -alumina may correspond to different migration paths of the aluminum atoms in neighboring domains during the γ to θ -alumina phase transition.

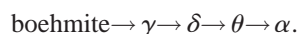
DOI: 10.1103/PhysRevB.67.224104

PACS number(s): 64.70.Kb, 81.30.Hd, 71.90.+q

I. INTRODUCTION

γ -alumina is an extremely important material in catalysis because of its porous structure with fine particle size, high surface area, and high catalytic surface activity. This material is widely used as a catalyst, an adsorbent, and as a support for industrial catalysts in hydrocarbon conversion¹⁻⁵ (petroleum refining), alcohol dehydration,⁶⁻⁸ the oxidation of organics,⁹⁻¹¹ the catalytic reduction of automotive pollutants such as nitric oxide (NO_x), and the oxidation of carbon monoxide (CO) and hydrocarbons.¹²⁻¹⁴ The broad technological importance of alumina has stimulated many investigations of its physical and chemical properties (see, e.g., Refs. 1-20).

Normally, γ -alumina is derived by thermal dehydration of aluminum hydroxide precursors. A typical and well-known sequence of dehydration reactions starts from boehmite ($\gamma\text{-AlOOH}$) and ends with hexagonal α -alumina,



γ -alumina is an intermediate product of this sequence of reactions and is metastable. At elevated temperatures (1000–1100 °C), undoped γ -alumina transforms rapidly to the more thermodynamically stable α -alumina phase. This process is accompanied by a catastrophic loss of porosity via sintering, and this fact negatively impacts the durability of γ -alumina when employed as a catalytic material. Stabilization of γ -alumina, therefore, is an extremely important industrial and commercial problem. Clearly, an understanding of the microscopic steps that comprise the mechanisms of the polymorphic phase transformations would be helpful in developing improved porous materials that could operate as catalysts at high temperatures without transforming to the less porous θ and α forms. Although many experimental and theoretical

investigations have been carried out to understand the catalytic properties of γ -alumina, heretofore the nature of the phase transformations in alumina has been very poorly understood, mostly because of poorly developed crystallinity in these materials.¹⁵ Furthermore, the continuous nature of the transformations between the forms during heating has made it difficult to probe such fine and irregular structures by traditional analytical techniques. Though high-resolution electron microscopy can reveal the crystallographic relations between the phases and provide clues to the transformation mechanisms, only a few high-resolution microscopy studies of the polymorphic phase transitions in alumina have been reported so far,¹⁹⁻²³ and the mechanisms of these transformations are still unclear. Therefore, theoretical investigations of the phase transitions in these materials that explain experimental phenomena would be very helpful.

In a recent paper²⁴ we demonstrated how the phase transition between γ - and θ -alumina may be investigated by using first-principles calculations and redefined unit cells. To the best of our knowledge, there was only one previous theoretical work related to the γ to θ -alumina transformation, which was reported by Levin and co-workers.^{16,23} They were trying to elucidate possible transformation paths using symmetry relationships and proposed a sequence of intermediate structures with different space groups that characterize the phase transition. They concluded that only aluminum atoms are reordered in such a transformation. Here we present a detailed atomistic description of the transformation from γ to θ -alumina. The mechanism described here predicts correctly the observed orientation relationship between γ - and θ -alumina, and naturally explains the origin of observed interfaces in domain boundaries in θ -alumina. The calculated rate of the thermal conversion between the two structures based on the proposed transformation mechanism is in an excellent agreement with the well-established experimental value.

The paper is organized as follows. In Sec. II we describe our computational approach in detail. Section III contains the description of the main calculations and results as well as a comparison of some predicted properties with the available experimental results. The central conclusions are summarized in Sec. IV.

II. COMPUTATIONAL METHOD

The theoretical results are based on density functional theory²⁵ calculations employing the PW91 generalized gradient approximation (GGA) to the exchange-correlation energy,^{26,27} as described in the review by Payne *et al.*²⁸ and coded in CASTEP. The electron-ion interactions were described by ultrasoft pseudopotentials.²⁹ We used a plane wave basis set with a cutoff energy of 380 eV to construct the (valence) electronic wave functions. A number of test calculations indicated that 380 eV is sufficient to obtain convergence in both the total energy differences and the geometries for the investigated systems. Integrations over the Brillouin zone employed a grid of k -points with a spacing of $0.1/\text{\AA}$ chosen according to the Monkhorst-Pack scheme.³⁰ Geometry optimization was considered to be converged when the difference of total energies between the last iterations did not exceed 2.0×10^{-5} eV/atom, and the rms (root mean square) displacement of atoms, the rms force on atoms, and the rms of the stress tensor were not higher than 1.0×10^{-3} \AA, 5.0×10^{-2} eV/\AA, and 1.0×10^{-1} Gpa, respectively. Vibrational frequencies of Al atoms were estimated in the harmonic approximation by diagonalizing the mass-weighted Cartesian force constant matrix for small displacements of the atom in question.³¹ The Cartesian force constants were calculated numerically from the second derivatives of the total energy E of the investigated configuration as follows:

$$\frac{\partial^2 E}{\partial x^2} \approx [E(x+\Delta x) - 2E(x) + E(x-\Delta x)]/(\Delta x)^2, \quad (1)$$

$$\frac{\partial^2 E}{\partial x \partial y} \approx \frac{[E(x+\Delta x, y+\Delta y) - E(x+\Delta x, y-\Delta y) - E(x-\Delta x, y+\Delta y) + E(x-\Delta x, y-\Delta y)]}{(4\Delta x \Delta y)}, \quad (2)$$

where x and y are arbitrary independent Cartesian nuclear coordinates. The step size for the numerical differentiation was taken as $\Delta x = \Delta y = 0.01$ \AA. The symmetry of the force constant matrix results in the requirement of sampling the total energy at 19 geometries. The theory and computational approach employed to determine the kinetics of aluminum migration in the bulk of alumina will be described in Sec. III.

III. RESULTS AND DISCUSSION

A. γ -alumina

γ -alumina has been described as a defect spinel structure (space group $Fd \bar{3} m$).^{15,32-35} Aluminum cations are distrib-

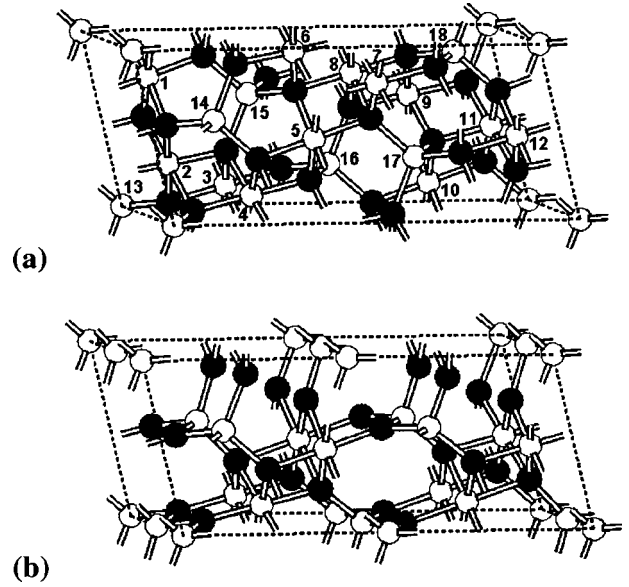


FIG. 1. (a) $\text{Al}_{16}\text{O}_{24}$ cell of γ -alumina defined by $\mathbf{a}_{\gamma_N} = 1.5\mathbf{a}_\gamma + 0.5\mathbf{b}_\gamma$, $\mathbf{b}_{\gamma_N} = -0.5\mathbf{b}_\gamma + 0.5\mathbf{c}_\gamma$, and $\mathbf{c}_{\gamma_N} = -0.5\mathbf{b}_\gamma - 0.5\mathbf{c}_\gamma$. Two of the 18 aluminum sites shown should be vacancies. (b) $\text{Al}_{16}\text{O}_{24}$ supercell of θ -alumina defined by $\mathbf{a}_{\theta_N} = \mathbf{a}_\theta - \mathbf{b}_\theta$, $\mathbf{b}_{\theta_N} = 2\mathbf{b}_\theta$, $\mathbf{c}_{\theta_N} = \mathbf{c}_\theta$, and the translation of cell origin (black spheres: oxygen; white spheres: aluminum). The similarity between them can be easily seen.

uted over the octahedral (O_h) and tetrahedral (T_d) interstitial sites (Wyckoff positions $16d$ and $8a$, respectively) defined by the face-centered-cubic (fcc) oxygen anion sublattice. 8/3 cation vacancies per cubic unit cell (one vacancy in every nine cation sites) are required to maintain the Al_2O_3 stoichiometry. Some studies have suggested a preference for aluminum cations in $8a$ positions,^{18,36-41} whereas other studies supported the opposite conclusion.^{18,35,40,42-46} There are also reports that suggest that Al can also occupy nonspinel sites.^{34,46,47} ²⁷Al NMR experiments show that $70 \pm 2\%$ of aluminum cations occupy octahedral interstitial sites,⁴⁸ in agreement with the value of $75 \pm 4\%$ reported earlier by John *et al.* in elegant temperature dependent experiments.⁴⁹ In practice, the vacancies are distributed in different sites of the cation sublattice. In this study, we assume that Al cations are distributed in $16d$ and $8a$ sites.

In order to investigate γ -alumina theoretically, one needs a unit cell with an integer number of vacancies and integer number of primitive formula units. Starting from a defect-free cubic spinel structure (AB_2O_4), there are multiple ways to construct a γ -alumina cell satisfying the above requirements. Here we define a unit cell $\text{Al}_{18}\text{O}_{24}$ ($\text{Al}_6\text{Al}_{12}\text{O}_{24}$ in the spinel notation) [Fig. 1(a)] in terms of the basis vectors of its cubic cell \mathbf{a}_γ , \mathbf{b}_γ and \mathbf{c}_γ , such that

$$\mathbf{a}_{\gamma_N} = 1.5\mathbf{a}_\gamma + 0.5\mathbf{b}_\gamma, \quad (3)$$

$$\mathbf{b}_{\gamma_N} = -0.5\mathbf{b}_\gamma + 0.5\mathbf{c}_\gamma, \quad (4)$$

$$\mathbf{c}_{\gamma_N} = -0.5\mathbf{b}_\gamma - 0.5\mathbf{c}_\gamma, \quad (5)$$

TABLE I. Optimized energies of γ -alumina with different vacancy configurations relative to θ -alumina.

Vacancy sites	Pure T_d			Pure O_h				
	15,18	15,17; 16,18	15,16; 16,17; 17,18	1,7; 1,8; 2,7; 2,8	2,6; 2,9; 6,9	1,6; 1,9	6,7; 6,8; 7,9; 8,9	1,2; 7,8
d (Å)	6.57	5.60	3.43	6.26	5.60	4.85	2.80	2.80
ΔE (eV/Al ₂ O ₃) ^a	0.35	0.54	0.57	0.15	0.32	0.24	0.52	0.70

$$^a \Delta E = E(\gamma) - E(\theta).$$

where \mathbf{a}_{γ_N} , \mathbf{b}_{γ_N} , and \mathbf{c}_{γ_N} are the unit vectors of the redefined cell. This is one of the smallest cells satisfying the requirements. The two vacancies can then be assigned to any two of the 18 cation sites to satisfy the Al₂O₃ stoichiometry. The lattice parameters of this newly defined cell Al₁₆O₂₄ (cell γ_N) can be calculated from the lattice parameters of cubic γ -alumina according to the above relationships between the two sets of unit vectors. When $a_\gamma = 7.918$ Å, $a_{\gamma_N} = 12.519$ Å, $b_{\gamma_N} = c_{\gamma_N} = 5.599$ Å, $\alpha_{\gamma_N} = 90^\circ$, and $\beta_{\gamma_N} = \gamma_{\gamma_N} = 102.92^\circ$. Clearly, b_{γ_N} and c_{γ_N} are equivalent.

First-principles calculations performed for the cell γ_N show that the total energy depends on the distribution of the two vacancies. Here we consider configurations with O_h (or T_d) vacancies only. The possible $16d$ ($8a$) sites in γ -alumina that are unoccupied in the model *A* of θ -alumina [see following sections and Fig. 3(a)] are the 1, 2, 6, 7, 8, and 9 (15, 16, 17, and 18) sites [Fig. 1(a)]. All configurations are fully relaxed, including atomic positions and cell dimensions. Five (three) different energies exist for different combinations of O_h (T_d) vacancy sites, (see Table I). As shown in Fig. 2, the energy increases with decreasing distance between the two vacancy sites, i.e., the lower energy states correspond to the more widely separated vacancies, in agreement with the conclusion of Wolverton and Hass.^{18,41} The slightly lower energy of the configuration with vacancies on sites 1,6 compared to that of sites 2,6 is due to more significant relaxation for atoms near vacancies. The energy difference between the optimized lowest and highest energy configurations is 0.55 eV/Al₂O₃, in reasonably good agreement with 0.33 eV/Al₂O₃ reported earlier from calculations using a similar computational method.¹⁸ Small deviations of this value may arise from different geometries of the cells used in the calculations. The energy of the lowest energy configura-

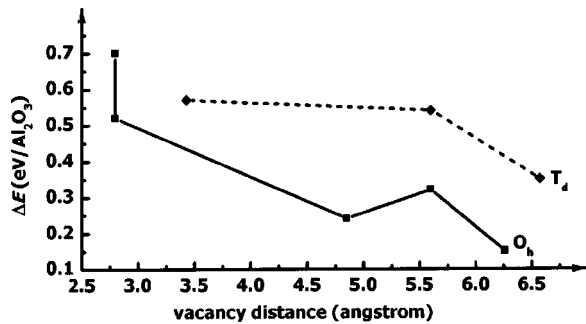


FIG. 2. Energy variation of optimized structure of γ -alumina relative to that of θ -alumina with vacancy separation.

tion with two O_h vacancies ($\gamma_N - O_h$) is 0.20 eV/Al₂O₃ lower than the lowest energy configuration with two T_d vacancies ($\gamma_N - T_d$), agreeing well with 0.24 eV/Al₂O₃ reported earlier.⁴¹ The vacancies of $\gamma_N - O_h$ locate on the $\{1\bar{1}\bar{1}\}_{\gamma_N}$ (i.e. $\{110\}_{\gamma}$) planes, in agreement with both the high resolution electron microscopy (HREM) observations^{44,45} and theoretical calculations.¹⁸

B. θ -alumina

θ -alumina is one of the few aluminas with well-known structure. It is reported to possess a monoclinic symmetry with the space group $C2/m$. There are 20 ions (four formula units) per unit cell with all of the ions located at $4i$ Wyckoff positions.^{34,35,50,51} The aluminum cations occupy four octahedral and four tetrahedral interstitials of the oxygen sublattice. Starting from the structure reported by Zhou *et al.*,³⁴ the total energy of optimized θ -alumina is 0.15–0.70 eV/Al₂O₃ lower than that of γ -alumina with pure T_d or O_h vacancies, depending on which vacancy distribution is assumed for γ -alumina (Table I).

C. Models of θ -alumina constructed from γ -alumina

Although γ - and θ -alumina have quite different structures (cubic and monoclinic symmetry, respectively), both of their oxygen anion sublattices are fcc, with aluminum cations occupying a portion of the available octahedral and tetrahedral interstices. Naturally, it is supposed that the phase transition of γ - to θ -alumina occurs by the migration of aluminum cations between the O_h/T_d interstitial sites available in the oxygen anion sublattice, which does not change appreciably during the γ - to θ -alumina transformation.¹⁶

Examining the θ structure carefully, we found that its primitive unit cell can be doubled to a cell with a shape very similar to that of γ_N [cell θ_N , Fig. 1(b)] by using new unit vectors

$$\mathbf{a}_{\theta_N} = \mathbf{a}_\theta - \mathbf{b}_\theta, \quad (6)$$

$$\mathbf{b}_{\theta_N} = 2\mathbf{b}_\theta, \quad (7)$$

$$\mathbf{c}_{\theta_N} = \mathbf{c}_\theta, \quad (8)$$

where \mathbf{a}_θ , \mathbf{b}_θ , and \mathbf{c}_θ are the basis vectors of θ -alumina, \mathbf{a}_{θ_N} , \mathbf{b}_{θ_N} , and \mathbf{c}_{θ_N} are the unit vectors of the θ_N supercell. Based on the experimental structure data and the above unit vector relationships,³⁴ $a_{\theta_N} = 12.20$ Å, $b_{\theta_N} = 5.808$ Å, c_{θ_N}

TABLE II. Comparison of structural parameters of θ -alumina.

Method	a (Å)	b (Å)	c (Å)	α (°)	β (°)	γ (°)	ΔE^a (eV/Al ₂ O ₃)	\bar{d} (Al _{O_h} -O) (Å)	\bar{d} (Al _{T_d} -O) (Å)
Expt. ^b	12.20	5.808	5.622	90	103.4	103.8	—	1.948	1.760
Expt. ^c	12.16	5.812	5.625	90	103.7	103.8	—	—	—
Expt. ^d	12.15	5.820	5.621	90	103.4	103.9	—	—	—
Expt. ^b (opt)	12.13	5.733	5.532	90.00	103.5	103.7	0	1.909	1.737
Model A (opt)	12.20	5.727	5.529	89.85	103.7	103.8	-0.002	1.912	1.738
Model B (opt)	12.22	5.719	5.529	89.90	103.6	103.8	0.0006	1.911	1.738
FLAPW (LDA) ^{e,f}	12.12	5.820	5.591	90	103.7	103.9	—	—	—
VASP (LDA) ^{e,f}	12.01	5.762	5.568	90	103.7	103.9	—	—	—
VASP (GGA) ^{e,f}	12.23	5.858	5.657	90	103.6	103.9	—	—	—
HF ^{f,g}	12.05	5.824	5.621	90	103.5	104.0	—	1.918	1.770

^a $\Delta E = E_{\text{exp}} - E_{\text{cal}}$. ^cReference 18.

^bReference 34. ^fLattice symmetry is kept unchanged during optimization.

^cReference 50. ^gReference 52.

^dReference 51.

=5.622 Å, $\alpha_{\theta_N} = 90^\circ$, $\beta_{\theta_N} = 103.4^\circ$, and $\gamma_{\theta_N} = 103.8^\circ$, as listed in Table II. Other experimental values are also converted according to the same relationships and listed in Table II for comparison. Clearly, the parameters of the γ_N -alumina unit cell are very close to those of θ_N -alumina. The \mathbf{a}_{θ_N} , \mathbf{b}_{θ_N} , and \mathbf{c}_{θ_N} correspond to \mathbf{a}_{γ_N} , \mathbf{b}_{γ_N} , and \mathbf{c}_{γ_N} , respectively. The oxygen sublattice of θ_N -alumina may be adjusted to one similar to the oxygen sublattice of γ_N -alumina by translating the origin of the new cell. The essential difference between γ_N and θ_N is, therefore, only in the distribution of Al atoms in the interstices among the fcc oxygen sublattice. The striking similarity between the structures can be seen in Fig. 1.

If Al atoms are assumed to move only to the adjacent unoccupied T_d or O_h sites, there are two different transformation schemes that transform the γ_N cell into a unit cell similar to θ_N . These two schemes give us two ways to convert the cell γ_N into a model of θ_N .

Scheme A: Keep two $8a$ and six $16d$ aluminum atoms at their original positions (assuming that there are no vacancies in these sites), and move the remaining eight aluminum atoms to two $16c$ and six $48f$ sites [below we refer the product of this scheme as model A; see Fig. 3(a)].

Scheme B: Keep two $16d$ aluminum atoms. All the 14 other aluminum atoms move to six $16c$, two $8b$ and six $48f$ sites [below we refer the product of this scheme as model B; see Fig. 3(b)].

Ignoring the slight distortion of the oxygen sublattice, the models A and B are translationally equivalent, with the translation vector $\mathbf{R} = \mathbf{c}_{\gamma_N}/2$ (Fig. 3). Each of the models A and B can be constructed in three equivalent ways. The three variants of the model A (or B) can be approximately (owing to the slight distortion of oxygen sublattice) generated from one of them by applying translation with the vectors $\mathbf{R} = \mathbf{a}_{\gamma_N}/6 - \mathbf{b}_{\gamma_N}/6 + \mathbf{c}_{\gamma_N}/3$ and $\mathbf{R} = \mathbf{a}_{\gamma_N}/3 + \mathbf{b}_{\gamma_N}/6 + 2\mathbf{c}_{\gamma_N}/3$. If the fractional coordinate of the oxygen anions in γ -alumina is taken to be 0.375 instead of the practical value 0.387,³³ the result-

ing θ models can be simplified to Al₈O₁₂ with structure similar to θ -alumina reported experimentally ($a' = 12.202$ Å, $b' = 2.799$ Å, $c' = 5.599$ Å, $\alpha' = \gamma' = 90^\circ$, $\beta' = 103.26^\circ$).

Based on the relationship of lattice axes between the γ_N -alumina and γ -alumina unit cells, the orientation relations between the γ -alumina and the θ -alumina models (no matter simplified or not) can be deduced to be $[010]_{\theta} \parallel [0\bar{1}1]_{\gamma}$ and $(100)_{\theta} \parallel (100)_{\gamma}$. According to the lattice symmetry, they are exactly equivalent to the experimental results of $[010]_{\theta} \parallel [110]_{\gamma}$ and $(100)_{\theta} \parallel (001)_{\gamma}$.^{16,23}

First-principles total-energy calculations and full geometry optimizations have been carried out for the two θ models described above and the experimental θ -alumina structure.³⁴ The geometric parameters and the related total energies are listed in Table II. Upon optimization, the two model structures and the experimental structure yield essentially identical structures. The cell parameters differ by less than 1%, and are consistent with earlier theoretical calculations.^{18,52} Energy differences are within 0.002 eV/Al₂O₃. The symmetries of the optimized structures of the two models and the experimental θ -alumina structure are all $C2/m$ within the limits of accuracy of the calculations. Average Al-O bond lengths are also very similar. (See Table II.) In general, all of these results indicate that the model structures considered above are equivalent to the experimental θ -alumina structure within the accuracy of the optimization procedure.

D. Transformation mechanism

Five possible nonequivalent fundamental steps exist for the migration of an Al cation in γ -alumina from its original interstitial site to a neighboring interstitial to form θ -alumina: (i) $8a$ to $16c$, (ii) $16d$ to $48f$, (iii) $8a$ to $48f$ (iv) $16d$ to $16c$, and (v) $16d$ to $8b$ (only for the scheme B). According to $Fd\bar{3}m$ symmetry, a $16c$ interstice has two nearest neighboring $8a$ sites. Every $48f$ site has one $8a$ and

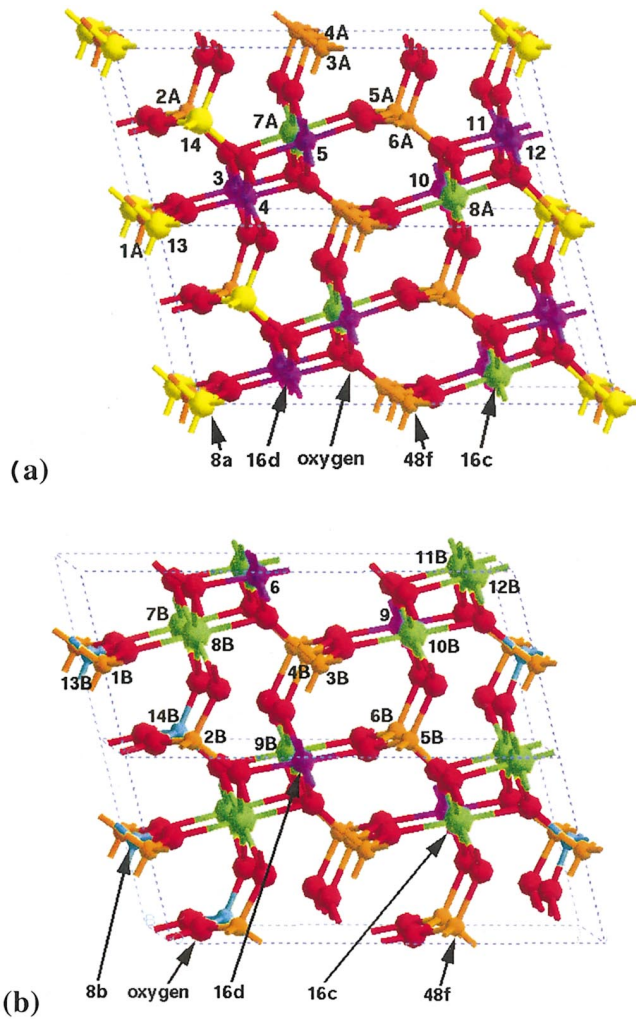


FIG. 3. (Color) Two θ models produced from γ -alumina by different transformation schemes: (a) Model A. (b) Model B. For easier comparison, two unit cells are shown. Note the translational relationship $\mathbf{R} = \mathbf{c}_\theta/2$ between the two models.

two $16d$ nearest neighbors. An $8b$ site has four adjacent $16d$ sites. Therefore, there are two, three, and four strong Al-Al repulsive interactions due to short Al-Al distance (shorter than 2.0 \AA , hereafter called an Al-Al bond) for an aluminum atom in a $16c$, $48f$ and $8b$ site, respectively, when no cation vacancies exist nearby.

In order to describe the overall phase transformation, we begin with calculations of intermediate configurations based on the motion of individual Al atoms. We then calculate the barriers of the individual steps and make some predictions for the kinetics of the phase transformation. First, let us consider the migration of one aluminum atom. The energy difference between the states before and after an aluminum moves depends on the initial and final positions of the moving atom as well as on the proximity of vacancies. The latter factor not only determines whether (and how many) strongly repulsive Al-Al bonds will be formed, but also the strength of the Al-O bonds that are broken and/or formed. Since the distribution of cation vacancies is uncertain,¹⁸ here we consider three situations: (I) No $8a/16d$ vacancies exist near the initial and final positions of the moving atom, i.e., all the oxygen atoms bound to the migrating aluminum atom and around the destination are four coordinated before the Al migration, and as many Al-Al bonds are formed as possible after the motion occurs. In this case, the influence of vacancies on the migration process can be ignored. (II) One $8a/16d$ vacancy is located near the destination of the moving atom thereby avoiding a stronger Al-Al repulsive interaction. The other vacancy is put far away from the initial and final positions of the moving atom so that its influence can be ignored. (III) Two $8a/16d$ vacancies are located in the vicinity of the final position of the moving atom so that one more Al-Al bond can be eliminated. In all the cases, the vacancies are all assigned to the sites unoccupied in model A (or B for the migration to $8b$ site). The calculated energies with the initial and final positions of migrating atoms, and the locations of vacancies are listed in Table III.

TABLE III. The energy variations caused by the migration of one aluminum atom per $\text{Al}_{16}\text{O}_{24}$ cell ($\text{eV}/\text{Al}_{16}\text{O}_{24}$).^a

	(I)			(II)			ΔE^o	(III)			ΔE^o
	Vac	Dir	ΔE	Vac	Dir	ΔE		Vac	Dir	ΔE	
$8a$ to $16c$	1,15	17-8A	10.16 (1)	15,18	16-7A	1.22 (0)	1.12 (0)	6,15	16-7A	-0.99 (0)	16 relax to 7A ^b
$16d$ to $48f$	1,14	9-5A	13.23 (2)	1,8	9-5A	5.28 (1)	0.65 (0)	8,17	9-5A	-1.19 (0)	16 toward 3B ^b
$8a$ to $48f$	2,15	17-6A	17.48 (2)	2,7	16-4A	9.07 (1)	4A back to $16c$	7,9	17-6A	-0.48 (0)	18 relax to 8A ^c
$16d$ to $16c$	1,13	7-7A	17.86 (2)	1,15	7-7A	7.98 (1)	7A relax to $15c$	15,16	7-7A	0.86 (0)	6 relax to 3A ^c
$16d$ to $8b$	17,18	3-14B	23.03 (3)	2,18	3-14B	11.82 (2)	14B relax to $2c$	2,4	3-14B	7.10 (1)	1.13 (0)

^a $\Delta E = E - E_0$, where E_0 and E are the energies of frozen initial and final configurations, respectively. $\Delta E^o = E^o - E_0^o$, where E_0^o and E^o are the energies of relaxed initial and final configurations, respectively. "Vac" indicates the locations of vacancies in initial configuration, "Dir" indicates the initial and final positions of migrating atoms, both refer to the labels of Figs. 1(a) and 3. Data in parentheses of ΔE and ΔE^o columns indicate the number of Al-Al bonds in the final configuration.

^bResulting from initial configuration.

^cResulting from final configuration.

To estimate the different energy variations in the numerous different cases, total energy calculations without structural relaxation were first carried out. The results show that the energy differences are all very large due to strong Al-Al repulsive interactions when no vacancies are around the destination. The energy differences decrease when the number of Al-Al bonds decreases. In case (III), some of the energy differences are negative, i.e., the final states are more stable than the initial ones. Thermodynamically spontaneous relaxation may occur in such cases. Based on these results, full optimization was performed for cases (II) and (III). In case (III), we find barrier-free relaxation of the $8a$ Al to the $16c$ site for the initial configuration of $8a$ to $16c$, similar to the result reported by Wolverton and Hass.¹⁸ For the initial state of $16d$ to $48f$, the $8a$ Al close to two vacancies goes toward a $16c$ site (deviation from $16c$ site is 0.58 \AA) after relaxation. The movement of an Al atom leads to the production of a new vacancy, which in turn gives rise to the migration of another Al atom, such as the cases of the final states of $8a$ to $48f$ and $16d$ to $16c$. For $8a$ to $48f$, the energy decrease reported with frozen structure is about $0.094 \text{ eV/Al}_2\text{O}_3$,¹⁸ which is close to our $0.48 \text{ eV/Al}_{16}\text{O}_{24}$. This spontaneous relaxation may be the reason for the occupation of non-spinel sites found in some x-ray and neutron refinements of γ - and η -alumina.^{34,46,47} For those structures without great change during geometry optimization, the strong Al-Al repulsive interactions also push Al atoms apart from each other in the relaxed structures, thus decreasing the energy [e.g., $16d$ to $8b$ in case (III), and $8a$ to $16c$ and $16d$ to $48f$ in case (II)]. In case (I), the aluminum atoms in $48f$ sites move back to a $16d$ site after geometry optimization of the final state of $16d$ to $48f$. While for case (II), the $48f$ Al tends to return to $8a$ site (0.75 \AA from $8a$) for the final state of $8a$ to $48f$; $16c$ Al relaxes to a $8a$ site for the final state of $16d$ to $16c$, and $8b$ Al relaxes to a $16d$ site for the final state of $16d$ to $8b$ due to the repulsion of the nearby Al atom.

Case (III) appears to provide the easiest route for aluminum migration, some steps of which may even happen spontaneously. As shown in Table I, however, there is an Al vacancy ordering tendency with widely separated vacancies being lower in energy than near-neighboring vacancies.¹⁸ Although the distribution of vacancies is practically determined by the process of thermal treatment, the energetic preference for widely separated vacancies renders the occurrence of two Al-vacancies located close to each other statistically improbable in a stable γ phase. Furthermore, more than two vacancies per γ_N cell are required if the transformation of γ - to θ -alumina is completely due to case (III), which is inconsistent with the stoichiometry. Therefore, the transformation of γ - to θ -alumina most probably starts from the migration of aluminum atoms with one vacancy nearby [case (II)].

As the energy cost of moving atoms depends on the locations of vacancies and the destinations, we took the lowest energy configuration $\gamma_N - O_h$ (vacancy sites: 2 and 7) as a start, and moved Al atoms to their destinations one by one to determine the lowest-energy intermediate states of scheme A. First, we tried moving each Al atom whose movement is required for the full transformation (atoms 1, 6, 8, 9, 15, 16, 17, and 18) to all of its possible destinations ($16c$ or $48f$).

From the energy differences between the initial and final configurations, we selected the lowest energy intermediate state. From this new state we continued the transformation by identifying the lowest energy displacement of a new Al atom until the model A structure was obtained. Total energy calculations were carried out first to identify the possible intermediate candidates at each step. Their structural parameters were then optimized except the lattice parameters (full relaxation gave similar results). The lowest energy sequence to complete the γ - to θ -alumina transformation was found to be six steps: (1) $6 \rightarrow 3A$, (2) $9 \rightarrow 6A$, (3) $16 \rightarrow 4A$, (4) $15 \rightarrow 7A$, (5) $1 \rightarrow 2A$, and (6) $18 \rightarrow 1A$. $17 \rightarrow 8A$ and $8 \rightarrow 5A$ were accomplished spontaneously accompanying the sixth step (Fig. 4). The calculated energies of intermediate states relative to $\gamma_N - O_h$ are indicated in Fig. 5.

On the basis of the above transformation sequence, we searched for the transition states between adjacent intermediates by successively fixing the position of the migrating atom and one of the atoms far away from it and relaxing all other atoms. (The second atom was chosen to be an atom that does not appreciably change its position in the initial and final intermediates. This prevents “sliding” of the entire unit cell.) The results are shown in Fig. 5. Step (4) is the rate-controlling step as its precursor is the highest energy intermediate with the highest energy peak to surmount.

As is the case in any chemical process involving a succession of increasingly energetic intermediates, the relative populations of the intermediates that precede the rate-controlling barrier depend on the temperature. As the temperature is increased, successively higher energy intermediates become populated. At sufficiently high temperature, the highest energy intermediate achieves appreciable population and formation of the product begins at a rate controlled by the barrier.

There are three factors that determine the rate at which a step takes place: the frequency with which reactant approaches the top of the barrier (transition state), the population of the reactant, and the probability that the reactant has sufficient energy to surmount the barrier. The rate is then given by

$$r = \nu f \rho(E > \Delta E), \quad (9)$$

where ν is the vibrational frequency corresponding to small oscillations around the equilibrium of the reactant structure, f is the population of the reactant, and $\rho(E > \Delta E)$ is the probability that the system has an energy greater than ΔE . The harmonic vibrational frequencies of the intermediate precursor to step (4) were calculated to be 2981, 3521, and 3839 cm^{-1} . Therefore, 3000 cm^{-1} was used to estimate the reaction rate of step (4). (The overall rate depends only linearly on ν but exponentially on ΔE , so small errors in the frequency have little impact on the predicted rate.) The probability $\rho(E > \Delta E)$ can be derived from the Boltzmann distribution. The Boltzmann distribution expresses the fraction of the number of particles (N) with energy E relative to the number of particles (N_0) with zero energy:

$$\frac{N}{N_0} = e^{-E/kT}, \quad (10)$$

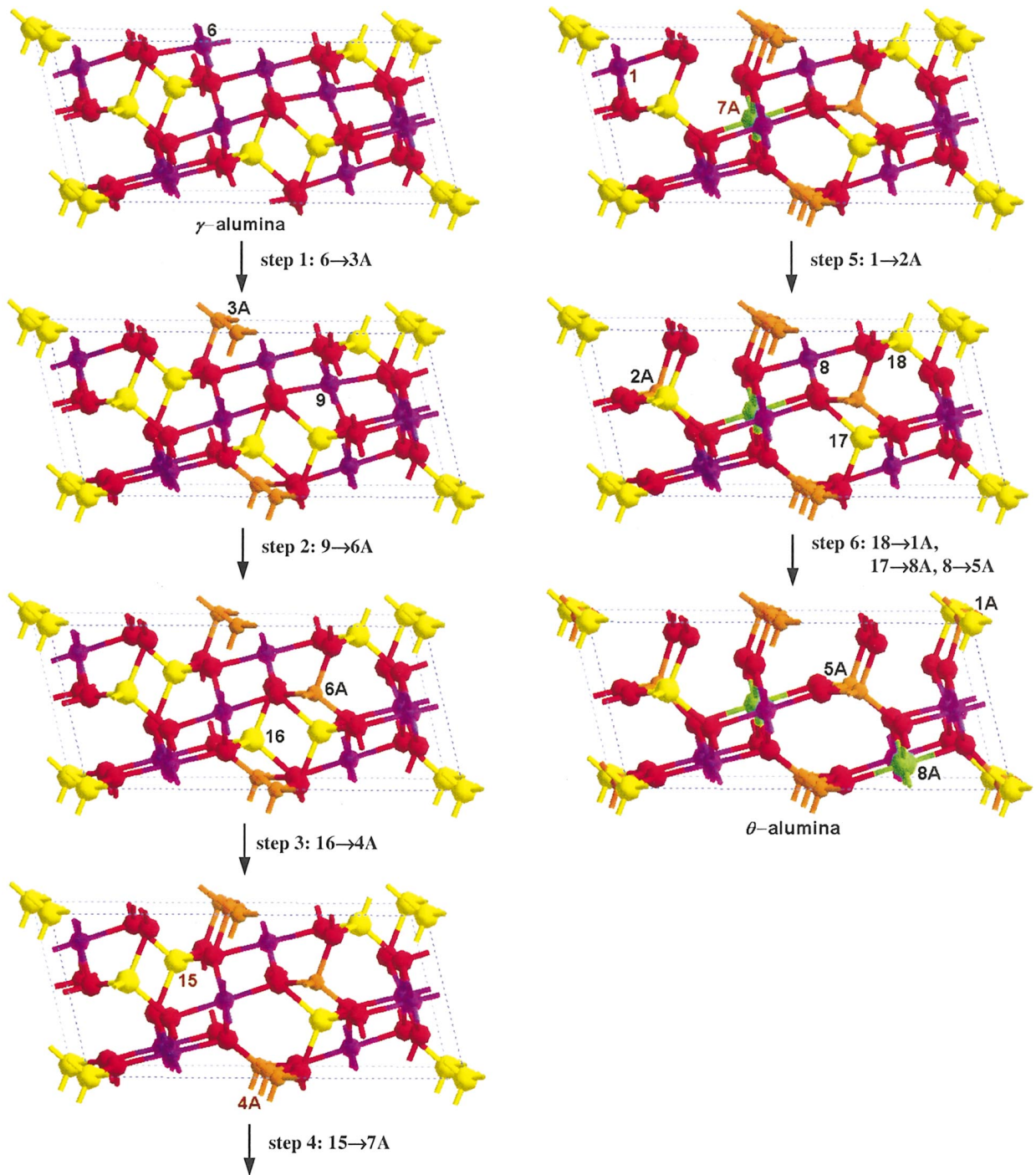


FIG. 4. (Color) Lowest energy transformation sequence of γ -alumina to θ -alumina by scheme A. Different color spheres represent oxygen atoms and aluminum atoms at different Wyckoff positions as indicated in Fig. 3.

here k is the Boltzmann constant and T is the temperature. Normalizing this distribution so that

$$\int_0^\infty N(E)dE = 1, \tag{11}$$

we obtain

$$N(E) = \frac{1}{kT} e^{-E/kT}. \tag{12}$$

Therefore, the probability $\rho(E > \Delta E)$ can be obtained from the integration of the above expression at the desired temperature

$$\rho(E > \Delta E) = \frac{1}{kT} \int_{\Delta E}^\infty e^{-E/kT} dE = e^{-\Delta E/kT}. \tag{13}$$

This form of rate analysis is well known from the nuclear decay theory⁵³ and has been successfully applied to compute

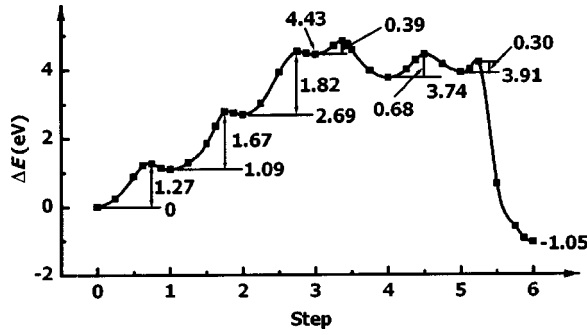


FIG. 5. Energy profile along the reaction pathway. The energy barriers for each step and the energies for each intermediate relative to the starting reactant are indicated.

the kinetics of hydrogen mobility in aluminas.⁵⁴ For step (4), ΔE is 0.39 eV.

Assuming that quasiequilibria among the reactant and intermediates that precede the rate-controlling step are achieved, one can employ the Boltzmann statistics to estimate the population of the intermediate precursor to the rate-controlling step,

$$f = \frac{e^{-E_3/kT}}{\sum_{i=0}^3 e^{-E_i/kT}}, \quad (14)$$

where E_i is the energy of the species i . The summation covers all the species that precede step (4). A pseudo-first-order kinetic description was then applied to this six-step sequence.

The temperature range of stability of the θ -alumina depends, among other factors, on the crystallinity of the initial material, on the presence of impurities, and on the thermal treatment procedure. Typically, it is about 1200–1300 K in the dehydration of boehmite.¹⁵ The predicted rate for the key step $i=4$ at 1300 K is $r = 1.76 \times 10^{-5} \text{ s}^{-1}$, implying that about 11 h are required for half of the reactants to surmount the barrier in the reaction step (4) [$(1-r)^\tau = 0.5$]. This reaction time is in excellent agreement with published experimental results (2–10 h).^{22,34,50}

Let us briefly consider the transformation scheme B . Table III shows that the energy increase accompanying the migration of Al(16d) to an $8b$ site is much higher than those of Al(16d) to $48f$ or $16c$ sites, which makes scheme B energetically less favorable than the scheme A . Furthermore, 14 atoms need to be reordered to complete the γ - to θ -alumina transformation by scheme B (instead of 8 atoms in the scheme A), rendering it statistically less probable as well. Therefore, for the same initial configuration, the transformation by the scheme B is much slower than the transformation by the scheme A . Of course, due to the statistical distributions of Al vacancies, numerous Al migration paths are possible, thus forming the variants of models A and B in different domains. This is consistent with the observed formation of twins and interfaces in θ -alumina.^{22,23}

E. Formation of domain boundaries

Both translational and rotational domain boundaries have been observed experimentally. The observed translational in-

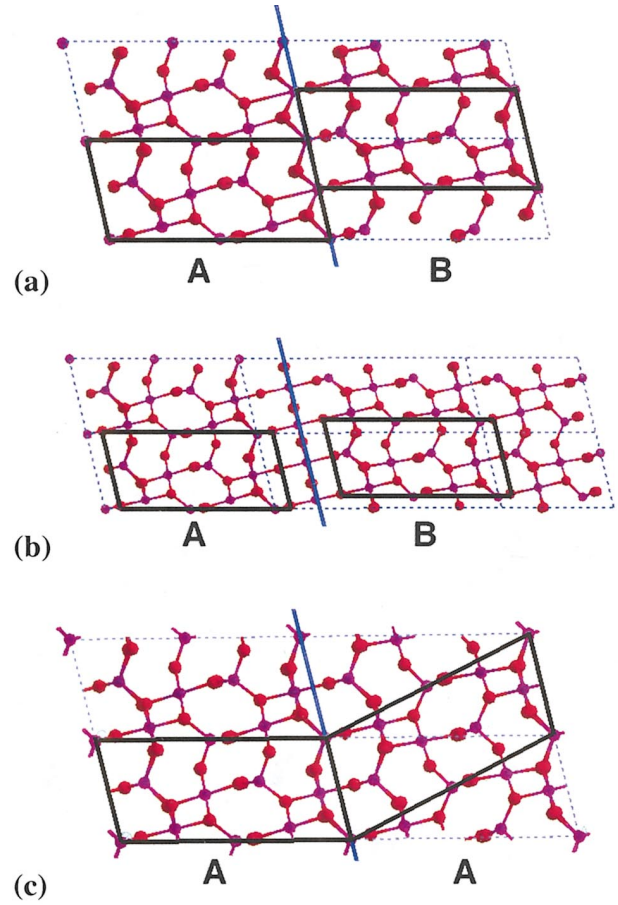


FIG. 6. (Color) Models of translational and rotational interfaces in θ -alumina: (a) Translational interface with $\mathbf{R} = \mathbf{c}_\theta/2$. (b) Translational interface with $\mathbf{R} = \mathbf{a}_\theta/3 + \mathbf{c}_\theta/6$. (c) Rotational interface with \mathbf{b}_θ and \mathbf{c}_θ rotates 180° around \mathbf{a}_θ .

terfaces are reported to correspond to the translation vectors $\mathbf{R} = \mathbf{c}_\theta/2$ and $\mathbf{R} = \mathbf{a}_\theta/3$.^{22,23} Based on above discussion, we see that the formation of translational interface with $\mathbf{R} = \mathbf{c}_\theta/2$ can be explained by ordering cations through schemes A and B respectively in neighboring domains [Fig. 6(a)].²³ However, the translational interface with $\mathbf{R} = \mathbf{a}_\theta/3$ seems to be incompletely identified.²³ According to the translational relationships between the variants of the θ models mentioned above, there are four other possible interfaces, with the vectors $\mathbf{R} = \mathbf{a}_{\gamma_N}/6 - \mathbf{b}_{\gamma_N}/6 + \mathbf{c}_{\gamma_N}/3$, $\mathbf{R} = \mathbf{a}_{\gamma_N}/6 - \mathbf{b}_{\gamma_N}/6 - \mathbf{c}_{\gamma_N}/6$, $\mathbf{R} = \mathbf{a}_{\gamma_N}/3 + \mathbf{b}_{\gamma_N}/6 + 2\mathbf{c}_{\gamma_N}/3$ and $\mathbf{R} = \mathbf{a}_{\gamma_N}/3 + \mathbf{b}_{\gamma_N}/6 + \mathbf{c}_{\gamma_N}/6$. Taking into account that $\mathbf{a}_{\gamma_N} = \mathbf{a}_\theta - \mathbf{b}_\theta$, $\mathbf{b}_{\gamma_N} = 2\mathbf{b}_\theta$, and $\mathbf{c}_{\gamma_N} = \mathbf{c}_\theta$, these relationships can be converted into $\mathbf{R} = \mathbf{a}_\theta/6 - \mathbf{b}_\theta/2 + \mathbf{c}_\theta/3$, $\mathbf{a}_\theta/6 - \mathbf{b}_\theta/2 - \mathbf{c}_\theta/6$, $\mathbf{R} = \mathbf{a}_\theta/3 + 2\mathbf{c}_\theta/3$, and $\mathbf{R} = \mathbf{a}_\theta/3 + \mathbf{c}_\theta/6$. Therefore, we suggest that the observed one is actually $\mathbf{R} = \mathbf{a}_\theta/3 + \mathbf{c}_\theta/6$, with the $\mathbf{c}_\theta/6$ value too small to be observed (near resolution limits) [Fig. 6(b)]. The rotational interface on the $(001)_\gamma$ planes can be obtained by the 180° rotation of the \mathbf{b}_{γ_N} and \mathbf{c}_{γ_N} axes around \mathbf{a}_{γ_N} , i.e., $\mathbf{a}'_{\theta_N} = \mathbf{a}_{\gamma_N}$, $\mathbf{b}'_{\theta_N} = -\mathbf{b}_{\gamma_N}$, $\mathbf{c}'_{\theta_N} = -\mathbf{c}_{\gamma_N}$ (in other word, $\mathbf{a}'_\theta = \mathbf{a}_\theta$, $\mathbf{b}'_\theta = -\mathbf{b}_\theta$, $\mathbf{c}'_\theta = -\mathbf{c}_\theta$) in a neighboring domain [Fig. 6(c)]. In such case the rotational interface is on $(100)_\theta$ planes. Because $(100)_\theta \parallel (100)_\gamma$ in our models, the interface on $(100)_\theta$ planes

is equivalent to the interface on $(100)_\gamma$ planes.²³ The interface of the twinning structures reported by Wang *et al.*²² actually includes both the rotational and translational components.

Levin and co-workers proposed a chain of maximal symmetry group/subgroup relation that connects the crystal structures of γ - and θ -alumina to explain the transformation process.^{16,23} To introduce $3/2a_\gamma$ for a lattice vector of θ -alumina, they suggested that the process must proceed through disordering of the γ form to a simple fcc structure with a_γ reduced by 2, and subsequent reordering with a threefold increase of the lattice parameter. This means that all the O_h (d and c) and T_d (a , b , and f) cation sites should first become equivalent as required by a fcc structure. Our study shows that $3/2a_\gamma$ may be easily explained by the θ models constructed from the γ_N cell. Although the $a_{\gamma_N} = (5/2)^{1/2}a_\gamma$, a_θ can be simplified to $3/2a_\gamma$ if the small distortion of the oxygen sublattice is neglected. It is possible that the lattice symmetry becomes nominally $Fm\bar{3}m$ during the γ - to θ -alumina transformation process by the scheme *B*, because of the large scale rearrangement on the Al sublattice and the involvement of $8b$ sites, but this restriction does not seem to be necessary in the domain where the transformation is achieved by scheme *A*, wherein the $8b$ sites are not involved.

IV. CONCLUSIONS

γ -alumina, a significant material in catalysis, transforms to θ -alumina at about 1200–1300 K. Although γ - and θ -alumina have quite different primitive unit cells, both of the structures can be described using $Al_{16}O_{24}$ unit cells that look very similar. This provides a clear framework for the investigation of the γ - to θ -alumina transformation. We found that once some of the aluminum atoms in γ -alumina move to specific neighboring interstitial sites, a close approximation of the θ -alumina structure is formed. Two different possible transformation schemes were proposed: scheme *A*, where eight aluminum atoms move from $16d/8a$ sites to two $16c$ and six $48f$ sites; scheme *B*, where fourteen aluminum atoms move from $16d/8a$ sites to six $16c$, six $48f$ and two $8b$ sites. In both cases the oxygen sublattice remains essentially unchanged. The structures of the θ models are translationally equivalent and are equivalent to the experimental structure of the θ -polytype within the accuracy of the optimization. The orientation relationships between γ - and θ -alumina suggested by these models agree with experimental observations.

Based on a comparison of the energy differences obtained from the first-principles calculations, the aluminum migra-

tion is proposed to take place first in the vicinity of cation vacancies to reduce the strong Al-Al interactions. As $8b$ sites are involved in scheme *B*, and Al atoms at $8b$ sites have one more strong Al-Al repulsive bond than those at $48f$ or $16c$ sites, scheme *B* is energetically less favorable than the scheme *A*. In addition, scheme *B* is statistically less probable, because six more Al atoms must be reordered in scheme *B* (than in the scheme *A*). Starting from the lowest energy configuration of γ -alumina, the lowest energy pathway of the transformation by scheme *A* was mapped out. The estimated conversion rate based on the potential energy profile along this pathway accurately predicts the experimental transformation temperature. The experimentally observed translational and rotational interfaces in θ -alumina can be attributed to different aluminum migration paths (resulting in models *A* and *B* and their variants) in neighboring domains during the γ - to θ -alumina transformation.

Our study not only explains well experimental observations, but also provides a detailed atomic-scale description of the phase transformation mechanism of γ -alumina to θ -alumina. From this mechanism, it is anticipated that the occupation of other elements in the cation vacancy sites or available interstitials ($48f$, $16c$, and $8b$) would be helpful to improve the thermal stability of γ -alumina at high temperatures which would greatly enhance its durability in catalytic applications. This is verified by the experiments which show that doping γ -alumina with traces of sodium or lanthanum species can effectively retard the transition of γ -alumina.^{34,55,56} However, doping elements should be carefully selected. Not all kinds of dopants have the same effect. Other factors such as interaction between dopant and alumina may change the role of dopants.^{57–59} For example, different mono-valent and divalent cations have different effect on the γ -alumina transformation.^{57,58} Furthermore, to maintain the catalytic activity, the influence of dopants on the specific surface area of γ -alumina should be considered.^{55–58} We anticipate that the atomic-scale description of the γ - to θ -alumina transformation mechanism provided here will help target doping studies.

ACKNOWLEDGMENTS

This work was supported in part by the U.S. DOE under Contract No. DE-FC02-01CH11085, by an NSF GOALI Grant No. DMR-0111841 with Alcoa, Inc., by the William A. and Nancy F. McMinn Endowment at Vanderbilt University, and by NNSF of China under Grant No. 10104011. Computations were partially supported by the National Center for Supercomputing Applications (NCSA) under Grant No. CHE990015Nr00 and utilized the SGI Origin2000 at NCSA, University of Illinois at Urbana-Champaign.

*Email address: sohlbergk@drexel.edu

¹H. Knözinger and P. Ratnasamy, *Catal. Rev. Sci. Eng.* **17**, 31 (1978).

²M. Che and C. O. Bennett, *Adv. Catal.* **36**, 55 (1989).

³Z. Xu, F.-S. Xiao, S. K. Purnell, O. Alexeev, S. Kawi, S. E. Deutsch, and B. C. Gates, *Nature (London)* **372**, 346 (1994).

⁴M. M. Ivey, H. C. Allen, A. Avoyan, K. A. Martin, and J. C.

Hemminger, *J. Am. Chem. Soc.* **120**, 10 980 (1998).

⁵M. Trombetta, G. Busca, S. Rossini, V. Piccoli, U. Cornaro, A. Guercio, R. Catani, and R. J. Willey, *J. Catal.* **179**, 581 (1998).

⁶H. Knözinger, *Angew. Chem., Int. Ed. Engl.* **7**, 791 (1968).

⁷B. Shi and B. H. Davis, *J. Catal.* **157**, 359 (1995).

⁸S. H. Cai and K. Sohlberg, *J. Mol. Catal. A: Chem.* **193**, 157 (2003).

- ⁹G. Busca, *Catal. Today* **27**, 457 (1996).
- ¹⁰V. S. Y. Lin, D. R. Radu, M. K. Han, W. H. Deng, S. Kuroki, B. H. Shanks, and M. Pruski, *J. Am. Chem. Soc.* **124**, 9040 (2002).
- ¹¹P. J. Kropp, G. W. Breton, J. D. Fields, J. C. Tung, and B. R. Loomis, *J. Am. Chem. Soc.* **122**, 4280 (2000).
- ¹²C. N. Satterfield, *Heterogeneous Catalysis in Practice* (McGraw-Hill, New York, 1980), Sec. 4.5.
- ¹³R. W. McCabe, R. K. Usmen, K. Ober, and H. S. Gandhi, *J. Catal.* **151**, 385 (1995).
- ¹⁴K. C. Taylor, *Catal. Rev. Sci. Eng.* **35**, 457 (1993).
- ¹⁵K. Wefers and C. Misra, *Oxides and Hydroxides of Aluminum*, Alcoa Technical paper No. 19 (Alcoa Laboratories, Pittsburgh, 1987).
- ¹⁶I. Levin and D. Brandon, *J. Am. Ceram. Soc.* **81**, 1995 (1998) and references therein.
- ¹⁷K. Sohlberg, S. J. Pennycook, and S. T. Pantelides, *Chem. Eng. Commun.* **181**, 107 (2000).
- ¹⁸C. Wolverton and K. C. Hass, *Phys. Rev. B* **63**, 024102 (2001) and references therein.
- ¹⁹I. Levin, Th. Gemming, and D. G. Brandon, *Phys. Status Solidi A* **166**, 197 (1998).
- ²⁰I. Levin and D. G. Brandon, *Philos. Mag. Lett.* **77**, 117 (1998).
- ²¹H. D. Santos, P. K. Kiyohara, and P. D. Santos, *Mater. Res. Bull.* **31**, 799 (1996).
- ²²Y. G. Wang, P. M. Bronsveld, J. T. M. De Hosson, B. Djuricic, D. McGarry, and S. Pickering, *J. Eur. Ceram. Soc.* **18**, 299 (1998).
- ²³I. Levin, L. A. Bendersky, D. G. Brandon, and M. Rühle, *Acta Mater.* **45**, 3659 (1997).
- ²⁴S. H. Cai, S. N. Rashkeev, S. T. Pantelides, and K. Sohlberg, *Phys. Rev. Lett.* **89**, 235501 (2002).
- ²⁵W. Kohn and L. J. Sham, *Phys. Rev.* **140A**, 1133 (1965).
- ²⁶J. P. Perdew, *Phys. Rev. B* **33**, 8822 (1986).
- ²⁷J. P. Perdew and Y. Wang, *Phys. Rev. B* **45**, 13244 (1992).
- ²⁸M. C. Payne, M. P. Teter, D. C. Allan, T. A. Arias, and J. D. Joannopoulos, *Rev. Mod. Phys.* **64**, 1045 (1992).
- ²⁹D. Vanderbilt, *Phys. Rev. B* **41**, 7892 (1990).
- ³⁰H. J. Monkhorst and J. D. Pack, *Phys. Rev. B* **13**, 5188 (1976).
- ³¹S. Califano, *Vibrational States* (Wiley, London, 1976).
- ³²E. J. W. Verwey, *Z. Kristallogr.* **91**, 317 (1935).
- ³³R. W. G. Wyckoff, *Crystal Structures* (Interscience Publishers, New York, 1963).
- ³⁴R.-S. Zhou and R. L. Snyder, *Acta Crystallogr., Sect. B: Struct. Sci.* **47**, 617 (1991), and references therein.
- ³⁵J. A. Wang, X. Bokhimi, A. Morales, O. Novaro, T. López, and R. Gómez, *J. Phys. Chem. B* **103**, 299 (1999).
- ³⁶V. Jayaram and C. G. Levi, *Acta Metall.* **37**, 569 (1989).
- ³⁷H. Saalfeld and B. B. Mehrotra, *Ber. Dtsch. Keram. Ges.* **42**, 161 (1965).
- ³⁸C. Pecharromán, I. Sobrados, J. E. Iglesias, T. González-Carreño, and J. Sanz, *J. Phys. Chem. B* **103**, 6160 (1999).
- ³⁹F. H. Streitz and J. W. Mintmire, *Phys. Rev. B* **60**, 773 (1999).
- ⁴⁰K. Sohlberg, S. J. Pennycook, and S. T. Pantelides, *J. Am. Chem. Soc.* **121**, 7493 (1999) and references therein.
- ⁴¹G. Gutierrez, A. Taga, and B. Johansson, *Phys. Rev. B* **65**, 012101 (2002).
- ⁴²K. P. Sinha and P. B. Sinha, *J. Phys. Chem.* **61**, 758 (1957).
- ⁴³H. Jagodzinski and H. Saalfeld, *Z. Kristallogr.* **110**, 197 (1958).
- ⁴⁴Y. G. Wang, P. M. Bronsveld, J. T. M. De Hosson, B. Djuricic, D. McGarry, and S. Pickering, *J. Am. Ceram. Soc.* **81**, 1655 (1998).
- ⁴⁵G. N. Kryukova, D. O. Klenov, A. S. Ivanova, and S. V. Tsybulya, *J. Eur. Ceram. Soc.* **20**, 1187 (2000).
- ⁴⁶V. A. Ushakov and E. M. Moroz, *React. Kinet. Catal. Lett.* **24**, 113 (1984).
- ⁴⁷F. Ernst, P. Pirouz, and A. H. Heuer, *Philos. Mag. A* **63**, 259 (1991).
- ⁴⁸M.-H. Lee, C.-F. Cheng, V. Heine, and J. Klinowski, *Chem. Phys. Lett.* **265**, 673 (1997).
- ⁴⁹C. S. John, N. C. M. Alma, and G. R. Hayes, *Appl. Catal.* **6**, 341 (1983).
- ⁵⁰G. Yamaguchi, I. Yasui, and W.-C. Chiu, *Bull. Chem. Soc. Jpn.* **43**, 2487 (1970).
- ⁵¹E. Husson and Y. Repelin, *Eur. J. Solid State Inorg. Chem.* **33**, 1223 (1996).
- ⁵²A. P. Borosy, B. Silvi, M. Allavena, and P. Nortier, *J. Phys. Chem.* **98**, 13 189 (1994).
- ⁵³D. Bohm, *Quantum Theory* (Prentice Hall, Englewood Cliffs, NJ, 1951).
- ⁵⁴K. Sohlberg, S. J. Pennycook, and S. T. Pantelides, *Recent Research Developments in Physical Chemistry* **4**, 71 (2000).
- ⁵⁵X. Y. Chen, Y. Liu, G. X. Niu, Z. X. Yang, M. Y. Bian, and A. He, *Appl. Catal., A* **205**, 159 (2001).
- ⁵⁶C. K. Loong, J. W. Richardson, and M. Ozawa, *J. Alloys Compd.* **250**, 356 (1997).
- ⁵⁷K. Okada, A. Hattori, Y. Kameshima, A. Yasumori, and R. N. Das, *J. Am. Ceram. Soc.* **83**, 1233 (2000).
- ⁵⁸K. Okada, A. Hattori, T. Taniguchi, A. Nukui, and R. N. Das, *J. Am. Ceram. Soc.* **83**, 928 (2000).
- ⁵⁹Y. Q. Wu, Y. F. Zhang, G. Pezzotti, and J. K. Guo, *Mater. Lett.* **52**, 366 (2002).